

N. Hansen, M. Braun-Unkhoff, T. Kathrotia, A. Lucassen, B. Yang
Understanding the Reaction Pathways in Premixed Flames Fueled by
Blends of 1,3-Butadiene and *n*-Butanol, Proc. Combust. Inst. 35 (2015) 771-778.

The original publication is available at www.elsevier.com

<http://dx.doi.org/10.1016/j.proci.2014.05.005/>

Understanding the Reaction Pathways in Premixed Flames Fueled by Blends of 1,3-Butadiene and *n*-Butanol

N. Hansen,^{1} M. Braun-Unkhoff,^{2*} T. Kathrotia,² A. Lucassen,¹ B. Yang³*

¹*Combustion Research Facility, Sandia National Laboratories, Livermore, CA 94551, USA*

²*German Aerospace Center (DLR), Institute of Combustion Technology, 70569 Stuttgart,
Germany*

³*Center for Combustion Energy and Key Laboratory for Thermal Science and Power
Engineering of Ministry of Education, Tsinghua University, Beijing, 100084, China*

accepted for oral presentation at the:

35th International Symposium on Combustion

Word Count (MS Word)

Abstract:	188
Introduction:	387
Experimental Procedures:	723
Combustion Chemistry Modeling:	273
Results and Discussion:	1375
Conclusions:	229
Acknowledgements:	176
41 References:	752
1 Table:	107
8 Figures: 191+158+342+165 +246+163+154+609=	2028
Total Words (excluding abstract):	6050

* Corresponding authors:
email: nhansen@sandia.gov (NH) and marina.braun-unkhoff@dlr.de

Abstract:

The oxidation of 1,3-butadiene/*n*-butanol flames was studied in a combined experimental and modeling work. The goal is to provide a detailed combustion chemistry model that allows for identification of the important pathways for butadiene and butanol oxidation as well as the formation of soot precursors and aromatics. Therefore, the chemical composition has been investigated for three low-pressure (20-30 torr) premixed flames, with different shares of butanol ranging between 25% to 75% compared to butadiene in 50% argon. Mole fraction profiles of reactants, products, and intermediates including C_3H_x and C_4H_x radicals as well as mono-aromatics such as benzyl radicals, were measured quantitatively as a function of height above burner surface employing flame-sampled molecular-beam mass spectrometry (MB-MS) utilizing photoionization with tunable vacuum-ultraviolet synchrotron radiation. The comparison of measured species profiles with modeling results provides a comprehensive view of the reaction model's quality and predictive capability with respect to the combustion chemistry of 1,3-butadiene and *n*-butanol under the current low-pressure, high-temperature conditions. In general, a good agreement was found between experimental and modeled results. Reaction flux and sensitivity analysis were used to get more insight into the combustion of the fuel.

1. Introduction

Over the last few years, global concerns over energy security and environmental degradation have resulted in a vital interest in the potential utilization of non-petroleum-based, *i.e.* bio-derived, fuels [1-4]. Especially the combustion characteristic of *n*-butanol has recently received a lot of attention in the combustion community and much experimental and modeling work has been done. As all the earlier insights cannot be reviewed here, the reader is referred to the comprehensive review by Sarathy *et al.* [5]. In summary, it is fair to say that our understanding of the combustion chemistry of *n*-butanol has advanced significantly over the last years and combustion chemistry models with predominant predictive capabilities can be generated [6-11].

With this major accomplishment in mind and realizing that *n*-butanol is likely not to be used as a single-component fuel but rather will be entered into the market as a blend with traditional petroleum-based fuels, it is now time to move our research focus on understanding the combustion chemistry in flames fueled by hydrocarbon/*n*-butanol blends. To this end, we have experimentally and theoretically studied the reaction pathways in flames fueled by blends of 1,3-butadiene and *n*-butanol. The goal of this study is to provide mechanistic insights into how the addition of *n*-butanol affects the small molecule species pool.

1,3-Butadiene is an interesting choice for the hydrocarbon component because (a) as a small di-ene, it can be regarded as a representative for this class of compounds in more realistic fuels, and (b) its consumption pathways are expected to lead to intermediates that differ from the ones formed in *n*-butanol oxidation steps [7, 12]. For example, the *i*-C₄H₅ and C₃H₃ radicals, which are likely key intermediates in the formation of the so-called “first aromatic ring” [13], are more readily formed in 1,3-butadiene than in *n*-butanol combustion processes. Generally

speaking, none of the commonly considered precursor species, like C_3H_3 , C_3H_5 , $i-C_4H_5$, or C_5H_5 , can be efficiently formed through n -butanol oxidation steps [6], and therefore it is not surprising that the addition of n -butanol to hydrocarbon flames can lead to a reduced concentration of soot and its precursors [14-17]. Such a trend is also observed in this study and the emphasis of this paper will be on how the small molecule chemistry changes based on the fuel blend composition and on the chemical insights gained from detailed kinetic modeling.

2. Experimental Procedures

In this paper, we report new experimental data in the form of isomer-resolved species mole fraction profiles of premixed flames fueled by three different 1,3-butadiene/ n -butanol blends. The flames, which were stabilized at a low pressure on a flat-flame McKenna burner, were analyzed using flame-sampling mass spectrometry with single-photon ionization. This part of the work was performed at the Chemical Dynamics Beamline of the Advanced Light Source of the Lawrence Berkeley National Laboratory [18].

The experimental set-up consists of the McKenna burner located in a low-pressure flame chamber, a quartz probe to sample gases from within the flames, a differentially pumped vacuum system, and a reflectron time-of-flight (TOF) mass spectrometer (MS). Compared to the previously used linear TOF MS [18], the improved mass resolution ($m/\Delta m \sim 3500$) now permits the separation of flame components based on their chemical composition. An example of the new flight-time resolution is shown in Fig. 1 for $m/z = 84$ of Flame 2 (see Table 1 and next paragraph for flame conditions). Based on our calibration, the three peaks indicate contributions of $C_4H_4O_2$, C_5H_8O , and C_6H_{12} isomers. It is immediately obvious that such a resolving capability is especially helpful when analyzing complex mixtures of oxygenated and hydrocarbon species

as they can be expected in a mixture of 1,3-butadiene and *n*-butanol flames.

The detailed flame conditions are summarized in Table 1. The gas flows of Ar, O₂, and 1,3-butadiene were controlled with calibrated mass flow controllers and the flow of the *n*-butanol was metered by a syringe pump, evaporated, and added quantitatively into the gas stream. The C/O ratio was kept constant for all three flames (C/O = 0.5), thus resulting in slightly different stoichiometries.

Details of the experimental and data reduction procedures are sufficiently described in the literature [18-22] and are not repeated here. In short, we used a quartz probe and a differentially pumped vacuum system to sample gases from within the three different flames and then used quasi-continuous beam of synchrotron-generated vacuum-ultraviolet (VUV) photons in the energy range of 8-17 eV as means to effectively ionize the sampled flame constituents. In a first step, we scanned the photon energy at a fixed burner position, which allowed us to record so-called photoionization efficiency (PIE) curves which were used to identify most of the compounds based on their characteristic ionization energies and PIE curves. While this is a very powerful technique, we have to keep in mind that especially for larger *m/z* ratios, this approach can become very complicated when potentially more isomers need to be separated and their ionization energies and PIE curves are unknown [19, 23-25].

Once the main components were all identified, we recorded mass spectra as a function of distance from the burner surface at fifteen different photon energies in order to provide the most reliable isomer-resolved mole fraction profiles possible. Mole fraction profiles of about 80 hydrocarbon and/or oxygenated species were determined for each flame. It is beyond the scope of this paper to discuss all profiles in detail and only a few will be discussed in the following Sections. However, all data, including the temperature profiles measured, are available in the

Supplementary Material or from the corresponding author (NH) upon request. As outlined in more details in Ref. [25], for most species' mole fractions an uncertainty of about 40% or less can be expected, but if the molecule's photoionization cross section is unknown even a larger error bar is conceivable. Uncertainties of $\pm 20\%$ are expected for the major species profiles. However, this level of experimental accuracy is adequate for testing and developing kinetic models. With regards to the sampling position, we estimate the uncertainty to be within ± 0.5 mm.

The temperature profiles were measured with laser-induced fluorescence (LIF) of the OH radical as described in Ref. [7]. Subsequently, the profiles were smoothed and used as input parameters in the modeling calculations. Concerning the accuracy of the temperature measurements, we estimate the uncertainty to be ± 150 K in the postflame and reaction zones and somewhat larger in the preheat zone where the OH concentrations are much smaller and the concentration and temperature gradients are much steeper. Again, this accuracy is still good enough to draw mechanistic conclusions, as shown earlier by Dooley *et al.* [26]. However, no attempts were made to evaluate potentially crucial rate parameters that could be sensitive to this temperature uncertainty.

3. Combustion Chemistry Modeling

The combustion chemistry model presented in this study consists of 216 species connected via 1028 reactions. A DLR reaction model shown earlier to describe the oxidation of low-pressure propene and cyclopentene flames [27, 28] was further enlarged; for details about the mechanism, see [27, 29, 30]. To describe the oxidation of 1,3-butadiene, recent work concerning the interaction between C_4H_6 isomers were revisited [31]. The details of the updates

are not provided here and instead the interested readers are referred to the Supplementary Material. The sub-model describing the butanol oxidation was gathered from Dagaut *et al.* [32] and adopted to the pressure range of this study. This model was chosen because it had the necessary level of details without being too large. In the present work, we have adopted the rate coefficients of unimolecular reactions within the butanol subsystem from Dagaut *et al.*, by reducing the *A*-factor by a constant factor of 4, with the value for the activation energy unchanged, to account for the pressure within the two studies. The full mechanism and all necessary parameters are given in the Supplementary Material.

Species profiles as a function of distance from the burner were calculated with the one-dimensional code PREMIX [33] using the experimentally determined flame temperature as input parameters, besides initial mass flow rates and composition of the reactants, and the burner's diameter as further input data. Thermal diffusion (Soret effect) was included in the model calculations. The species transport was considered using the multicomponent transport model. For the species involved, transport data were taken from the CHEMKIN transport database [34], thermodynamic data from Ref. [35] or evaluated with group additivity rules [36].

4. Results and Discussion

Insights into the reaction paths within these three flames can be gained from comparing the experimentally determined chemical structure of the flames with each other or from comparing them to the results of the model calculations. For the latter approach it is worth noting that besides the maximum mole fraction, the profile shapes and peak positions are also valuable for testing the quality of the reaction model. Such a comparison between experimental and modeling results provides a comprehensive view of the capabilities of the reaction model to

predict the ongoing chemistry under the chosen conditions. Most predicted mole fraction profiles are in good agreement with the experimentally observed profiles, thus, allowing a reaction flux and sensitivity analysis to investigate the importance of consumption pathways of the educts. Our main findings are discussed in the next paragraphs.

The comparison between predicted and measured major species profiles (H_2 , H_2O , CO , O_2 , Ar , CO_2 , C_4H_6 , *n*-butanol) is shown in Fig. 2 for Flame 2. Clearly, the model results match the major species profiles within the expected uncertainties. Similar levels of agreement were found for Flame 1 and Flame 3. Some discrepancies between experiment and model results occur near the burner surface, where probe perturbation and uncertainties of the temperature profiles are known to have some effects [37].

Furthermore, the model is also able to describe the formation and consumption of most C_1 , C_2 , and C_3 species. As an example, Fig. 3 shows the experimental and modeled mole fractions of CH_3 , C_2H_4 , and C_3H_4 (allene) for all three flames, and in general, these species' profiles are reproduced accurately by the model with respect to amount and shape. Somewhat larger discrepancies have been observed for ethane which is underpredicted by about a factor of four. We also note that differences in the peak mole fractions of CH_3 and C_2H_4 (C_1 and C_2 species in general) exist between all three flames, in predictions and experiments, and that these differences are minor for the C_3 species. Indeed, allene mole fractions are almost the same for all three flames (both in model predictions and experimental results). A reason for this unexpected result cannot be provided at this point. Furthermore, a trend can be seen for mole fractions of C_2 and C_4 species. That is, C_2 species are more present in the flame containing more *n*-butanol (Flame 3), while C_4 intermediates (not shown) are present in higher abundances in Flame 1. This effect can probably be traced back to the different fuel-decomposition pathways. Also, the

differences between measured and calculated mole fractions are larger for Flame 3, *i.e.* under a more fuel rich condition. These findings reflect the close relationship of CH_x radicals and the chemistry of stable C_2 intermediates.

The reaction model used is also capable of describing the formation and consumption of acetylene (C_2H_2), one of the most important molecules with respect to the formation of aromatic species and soot, and of vinyl (C_2H_3) and ethyl (C_2H_5) radicals, according to Fig. 4. However, ethyl radicals are predicted to peak closer to the burner's surface than experimentally observed.

The C_4H_x ($x=2-5$) intermediates are direct oxidation products of 1,3-butadiene, as also revealed by reaction flux analysis visualized later, and not surprisingly, when this fuel is replaced with *n*-butanol, the concentration of these intermediates decreases as well. At the same time, mole fractions of *n*-butanol specific oxidation products, like butenols and butanal increase when *n*-butanol is added to a 1,3-butadiene flame. No example is shown explicitly in this paper and instead the focus is shifted on the formation of aromatic species, and their precursors, as C_4H_x species are known to be able to take part in the formation routes of benzene and phenyl [12].

Figure 5 shows, for Flame 2, a comparison of the experimental and modeled mole fractions of the benzene precursors C_3H_3 , C_3H_5 , and C_4H_5 . While the overall peak heights are predicted quite accurately for the C_3H_3 and C_3H_5 radicals, the level of C_4H_5 radicals is overpredicted by more than an order of magnitude. Also, the predicted profile for C_4H_5 seems to peak slightly earlier than observed in the experiment; the opposite is true for the C_3H_3 radical. Based on our previous work [12, 38] and the PIE curves measured in this study, it is expected that the resonance stabilized radicals *i*- C_4H_5 , CH_3CHCCH , and CH_3CCCH_2 are the main contributors. Only the *i*- and the *n*- C_4H_5 are included in the model, with the model predicting the *i*-form to accumulate in larger concentrations (by about a factor of 10). The observed ratios of

the peak mole fractions of benzene to propargyl are within the expected range for these flame conditions as Hansen *et al.* have shown in a comparison of available literature data [39].

Major oxygen-containing intermediates in the oxidation of the investigated flames are given in Fig. 6, where experimental and calculated mole fraction profiles of two small aldehydes (formaldehyde - CH_2O ; acetaldehyde - CH_3CHO) and an aromatic alcohol (phenol - $\text{C}_6\text{H}_5\text{OH}$) are plotted. In general, a good agreement is seen, with respect to height and shape, in particular for acetaldehyde and phenol, although the formaldehyde level is under predicted by up to a factor of two; in addition, its profile is predicted broader compared to the measured one. Concerning alcoholic molecules, the measured mole fractions of methanol are in the order of 4×10^{-4} , with predictions even smaller. Ethanol ($m/z = 46$) was not observed in the experimental work.

A comparison of further one ring aromatics is depicted in Fig. 7, for toluene (C_7H_8), with about 20 ppm the highest concentrations, and benzyl radicals (C_7H_7), and styrene (C_8H_6), with peak concentrations measured up to about 2 ppm. In general, the simulated profiles are considerably smaller; thus indicating that the model has to be updated to better match the experimental results. For example, it is possible that the above mentioned CH_3CHCCH , and CH_3CCCH_2 radicals react with propargyl to form benzyl+H/toluene in a reaction similar to the $\text{C}_3\text{H}_3 + \text{C}_3\text{H}_3$ recombination. However, the relative ratio in the concentrations to each other is matched.

Reaction-path and sensitivity analysis were performed to identify the dominant mechanistic pathways for the consumption of the reactants of the fuel as well as for the formation and consumption of major intermediates and to see where more accurate rate coefficients might be required. The results for all flames will be discussed next.

The rate of production is shown in Fig. 8 where the consumption of 1,3-butadiene to form

benzene precursors such as acetylene and propargyl radicals is presented for all three flames, at 3 mm above the burner's surface. Consumption of 1,3-butadiene in all three flames is dominated by forming *iso*-butadienyl radical (*i*-C₄H₅) in addition to small channels leading to *n*-C₄H₅ or acetylene. In another small channel 1,3-butadiene forms allyl radicals which further form mainly C₃H₆ and C₃H₃ (propargyl radicals) via propyne and allene. Both, the *i*- and the *n*-isomers of the butadienyl radicals are consumed to form mainly vinylacetylene. The reaction channel of *n*-C₄H₅ to C₄H₄ is more prominent in Flame 1 compared to Flame 2. Diacetylene (C₄H₂) is subsequently formed via C₄H₃ as main pathway. In its secondary channel, *i*-C₄H₅ leads to the formation of propargyl radicals which is the major precursor to benzene formation. The propargyl (C₃H₃) recombination reaction leads to about 50% benzene formation, as the major pathway. In addition, *n*-butadienyl radical in a reaction with acetylene is responsible for about 15-25% benzene formation. It was shown in Refs. [12, 40] that the *i*-C₄H₅+C₂H₂ and C₃H₃+C₃H₅ reactions can contribute to the overall aromatic ring formation via fulvene as an intermediate. However, fulvene reactions, including the H-assisted isomerization to benzene [41], are currently not included in the model. A reaction channel of phenyl radical with H atom is found prominent only in Flame 1, whereas reactions from styrene and toluene contribute less than 5%.

The sensitivity analysis reveals that the overall performance of the reaction model depends mainly on the rates of H-abstraction reactions. The well-known reactions of the HCO and H/O-system, namely the chain branching reactions $\text{H}+\text{O}_2 \rightleftharpoons \text{OH}+\text{O}$ and $\text{HCO}+\text{M} \rightleftharpoons \text{H}+\text{CO}+\text{M}$, are the most important ones, in addition to H abstraction reactions of the fuel molecules. For the intermediates, such as propargyl and benzene, reactions of C₄H_x and C₃H_x species and of propargyl recombination, are the most sensitive ones.

5. Conclusions

In the present study, results of a combined modeling and experimental effort to study oxidation of a three 1,3-butadiene/*n*-butanol flame/Ar were presented, at a low-pressure flat flame condition. An alcohol based flame combined with butadiene was used to investigate in the formation of aromatics and their precursors when hydrocarbons are blended in alcohols. The chemical kinetic model presented in this work was based on an earlier kinetic model depicting oxidation of 1,3-butadiene, propene, and cyclopentene flames and has been extended to include chemistry of *n*-butanol.

The flame structures of 1,3-butadiene/*n*-butanol flames were measured experimentally employing flame-sampled molecular-beam mass spectrometry which provides species profiles identified and separated by their characteristics ionization energies. The uncertainty of mole fractions measured was estimated to be about 40% and with respect to sampling position, to be within ± 0.5 mm. Among many hydrocarbon and/or oxygenated species measured, only profiles of important intermediates such as C_2H_x (vinyl, ethyl, acetylene), C_3 -species (propargyl, allene), C_4H_x intermediates (C_4H_5 radicals) and other benzene precursors are presented, besides the ones for educts and major products. A comparison between experimental and model results demonstrated reasonably good agreement. In general, benzene formation is proportional to the amount of butadiene in the fuel, and the propargyl recombination reaction is the major path responsible for benzene formation in addition to *n*-butadienyl radicals. Future work will address the role of larger aromatics, including indene and naphthalene.

Acknowledgments

The work is supported by the DAAD (Deutscher Akademischer Austausch Dienst) under Grant No. 56025647. NH and AL are supported by the U.S. Department of Energy (USDOE), Office of Basic Energy Sciences (BES) under Grand No. DE-AC04-94-AL85000 and DE-SC0001198 (the Energy Frontier Research Center for Combustion Science). BY is supported by National Science Foundation of China (51306102) and the "National 1000 Young Talents Program" of China. MBU and TK are grateful to the assistance of S. Asenbauer, T. Brandes, and L. Cordes in the modeling work and preparing plots. The measurements were performed within the "Flame Team" collaboration at the Advanced Light Source (ALS), Lawrence Berkeley National Laboratory, Berkeley, USA, and we thank the students and postdocs for the help with the data acquisition. The experiments have profited from the expert technical assistance of Paul Fugazzi. The Advanced Light Source is supported by the Director, Office of Science, BES, USDOE under Contract No. DE-AC02-05CH11231. Sandia is a multi-program laboratory operated by Sandia Corporation, a Lockheed Martin Company, for the National Nuclear Security Administration under contract DE-AC04-94-AL85000.

References:

- [1] K. Kohse-Höinghaus, P. Oßwald, T. A. Cool, T. Kasper, N. Hansen, F. Qi, C. K. Westbrook, P. R. Westmoreland, *Angew. Chem. Int. Ed.* 49 (21) (2010) 3572-3597.
- [2] T. Kick, J. Herbst, T. Kathrotia, J. Marquetand, M. Braun-Unkhoff, C. Naumann, U. Riedel, *Energy* 43 (1) (2012) 111-123.
- [3] A. Mzé Ahmed, P. Dagaut, K. Hadj-Ali, G. Dayma, T. Kick, J. Herbst, T. Kathrotia, M. Braun-Unkhoff, J. Herzler, C. Naumann, U. Riedel, *Energy Fuels* 26 (10) (2012) 6070-6079.
- [4] P. Dagaut, F. Karsenty, G. Dayma, P. Diévert, K. Hadj-Ali, A. Mzé Ahmed, M. Braun-Unkhoff, J. Herzler, T. Kathrotia, T. Kick, C. Naumann, U. Riedel, L. Thomas, *Combust. Flame* 161 (3) (2013) 835-847.
- [5] S. M. Sarathy, P. Oßwald, N. Hansen, K. Kohse-Höinghaus, *Prog. Energy Combust. Sci.* in press, [dx.doi.org/10.1016/j.pecs.2014.04.003](https://doi.org/10.1016/j.pecs.2014.04.003) (2014).
- [6] S. M. Sarathy, S. Vranckx, K. Yasunaga, M. Mehl, P. Oßwald, W. K. Metcalfe, C. K. Westbrook, W. J. Pitz, K. Kohse-Höinghaus, R. X. Fernandes, H. J. Curran, *Combust. Flame* 159 (6) (2012) 2028-2055.
- [7] N. Hansen, M. R. Harper, W. H. Green, *Phys. Chem. Chem. Phys.* 13 (45) (2011) 20262-20274.
- [8] A. Frassoldati, R. Grana, T. Faravelli, E. Ranzi, P. Osswald, K. Kohse-Höinghaus, *Combust. Flame* 159 (7) (2012) 2295-2311.
- [9] J. H. Cai, L. D. Zhang, F. Zhang, Z. D. Wang, Z. J. Cheng, W. H. Yuan, F. Qi, *Energy Fuels* 26 (9) (2012) 5550-5568.
- [10] M. R. Harper, K. M. Van Geem, S. P. Pyl, G. B. Marin, W. H. Green, *Combust. Flame* 158 (1) (2011) 16-41.
- [11] K. Yasunaga, T. Mikajiri, S. M. Sarathy, T. Koike, F. Gillespie, T. Nagy, J. M. Simmie, H. J. Curran, *Combust. Flame* 159 (6) (2012) 2009-2027.

- [12] N. Hansen, J. A. Miller, T. Kasper, K. Kohse-Höinghaus, P. R. Westmoreland, J. Wang, T. A. Cool, *Proc. Combust. Inst.* 32 (2009) 623-630.
- [13] N. Hansen, J. A. Miller, S. J. Klippenstein, P. R. Westmoreland, K. Kohse-Höinghaus, *Combust. Expl. Shock* 48 (5) (2012) 508-515.
- [14] G. S. Chen, Y. G. Shen, Q. C. Zhang, M. F. Yao, Z. Q. Zheng, H. F. Liu, *Energy* 54 (2013) 333-342.
- [15] L. Siwale, L. Kristof, T. Adam, A. Bereczky, M. Mbarawa, A. Penninger, A. Kolesnikov, *Fuel* 107 (2013) 409-418.
- [16] H. Wang, R. D. Reitz, M. F. Yao, B. B. Yang, Q. Jiao, L. Qiu, *Combust. Flame* 160 (3) (2013) 504-519.
- [17] Q. C. Zhang, M. F. Yao, Z. Q. Zheng, H. F. Liu, J. Xu, *Energy* 47 (1) (2012) 515-521.
- [18] T. A. Cool, A. McIlroy, F. Qi, P. R. Westmoreland, L. Poisson, D. S. Peterka, M. Ahmed, *Rev. Sci. Instr.* 76 (9) (2005) 094102.
- [19] N. Hansen, T. A. Cool, P. R. Westmoreland, K. Kohse-Höinghaus, *Prog. Energy Combust. Sci.* 35 (2) (2009) 168-191.
- [20] P. Osswald, U. Struckmeier, T. Kasper, K. Kohse-Höinghaus, J. Wang, T. A. Cool, N. Hansen, P. R. Westmoreland, *J. Phys. Chem. A* 111 (19) (2007) 4093-4101.
- [21] T. A. Cool, K. Nakajima, C. A. Taatjes, A. McIlroy, P. R. Westmoreland, M. E. Law, A. Morel, *Proc. Combust. Inst.* 30 (2005) 1681-1688.
- [22] F. Qi, *Proc. Combust. Inst.* 34 (2013) 33-63.
- [23] N. Hansen, S. J. Klippenstein, J. A. Miller, J. Wang, T. A. Cool, M. E. Law, P. R. Westmoreland, T. Kasper, K. Kohse-Höinghaus, *J. Phys. Chem. A* 110 (13) (2006) 4376-4388.
- [24] N. Hansen, S. J. Klippenstein, P. R. Westmoreland, T. Kasper, K. Kohse-Höinghaus, J. Wang, T. A. Cool, *Phys. Chem. Chem. Phys.* 10 (3) (2008) 366-374.

- [25] F.N. Egolfopoulos, N. Hansen, Y. Ju, K. Kohse-Höinghaus, C. K. Law, F. Qi, *Progr. Energy Combust. Sci.* in press, doi:10.1016/j.pecs.2014.04.004 (2014).
- [26] S. Dooley, F. L. Dryer, B. Yang, J. Wang, T. A. Cool, T. Kasper, N. Hansen, *Combust. Flame* 158 (4) (2011) 732-741.
- [27] M. Kamphus, M. Braun-Unkhoff, K. Kohse-Höinghaus, *Combust. Flame* 152 (1-2) (2008) 28-59.
- [28] M. Köhler, A. Brockhinke, M. Braun-Unkhoff, K. Kohse-Höinghaus, *J. phys. Chem. A* 114 (14) (2010) 4719-4734.
- [29] H. Böhm, M. Braun-Unkhoff, P. Frank, *Prog. Comput. Fluid Dyn.* 3 (2003) 145-150.
- [30] H. Böhm, M. Braun-Unkhoff, *Combust. Flame* 153 (2008) 84-96.
- [31] S. Peukert, C. Naumann, M. Braun-Unkhoff, *Z. Phys. Chem.* 223 (4-5) (2009) 427-446.
- [32] P. Dagaut, S. M. Sarathy, M. J. Thomson, *Proc. Combust. Inst.* 32 (2009) 229-237.
- [33] R.J. Kee, F.M. Rupley, J. A. Miller, 1992 "PREMIX: One-dimensional premixed laminar flame code, CHEMKIN-II Version 2.5b", Sandia Laboratories, Livermore, CA, USA.
- [34] R.J. Kee, G. Dixon-Lewis, J. Warnatz, M.E. Coltrin, J. A. Miller, 1986, "The Chemkin Transport Database. Report SAND86-8246", Sandia National Laboratories, Livermore, CA, USA.
- [35] R.J. Kee, F.M. Rupley, J. A. Miller, 1987, "CHEMKIN: The Chemkin Thermodynamic Database. Rep. SAND87-8215", Sandia National Laboratories, Livermore, CA, USA.
- [36] S. W. Benson, F. Cruicksh, D. M. Golden, G. R. Haugen, H. E. Oneal, A. S. Rodgers, R. Shaw, R. Walsh, *Chem. Rev.* 69 (3) (1969) 279-&.
- [37] U. Struckmeier, P. Oßwald, T. Kasper, L. Bohling, M. Heusing, M. Köhler, A. Brockhinke, K. Kohse-Höinghaus, *Z. Phys. Chem.* 223 (4-5) (2009) 503-537.

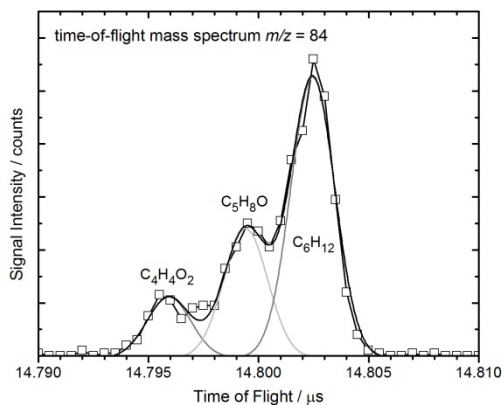
- [38] N. Hansen, S. J. Klippenstein, C. A. Taatjes, J. A. Miller, J. Wang, T. A. Cool, B. Yang, R. Yang, L. X. Wei, C. Q. Huang, F. Qi, M. E. Law, P. R. Westmoreland, J. Phys. Chem. A 110 (10) (2006) 3670-3678.
- [39] N. Hansen, T. Kasper, B. Yang, T. A. Cool, W. Li, P. R. Westmoreland, P. Oßwald, K. Kohse-Höinghaus, Proc. Combust. Inst. 33 (2011) 585-592.
- [40] N. Hansen, W. Li, M. E. Law, T. Kasper, P. R. Westmoreland, B. Yang, T. A. Cool, A. Lucassen, Phys. Chem. Chem. Phys. 12 (38) (2010) 12112-12122.
- [41] A. W. Jasper, N. Hansen, Proc. Combust. Inst. 34 (2013) 279-287.

Table 1: (107 words)**Flame Conditions**

	ϕ^a	Cold Gas Composition (%)				Pressure (Torr)	Cold Gas Velocity (cm ⁻¹)
		Ar	1,3-Butadiene	<i>n</i> -Butanol	O ₂		
Flame 1	1.45	50.0	7.7	2.6	39.7	20	97.7
Flame 2	1.53	50.0	5.3	5.3	39.5	20	97.7
Flame 3	1.62	50.0	2.7	8.1	39.2	30	65.1

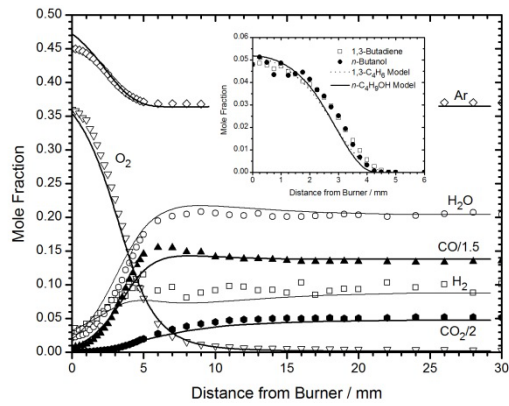
^{a)} stoichiometry

Figure 1: $(54.9+10) \times 2.2 + 26 = 191$ words



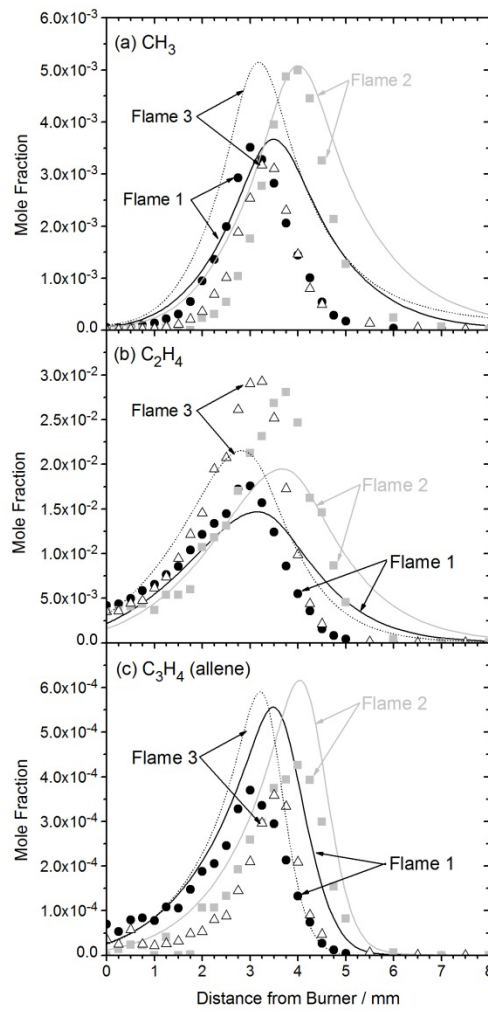
Visible demonstration of the mass spectrometer's resolving capabilities. Species with the molecular composition of $\text{C}_4\text{H}_4\text{O}_2$, $\text{C}_5\text{H}_8\text{O}$, and C_6H_{12} contribute to the signal at the nominal $m/z=84$.

Figure 2: (53.3+10)x2.2=139+19=158 words



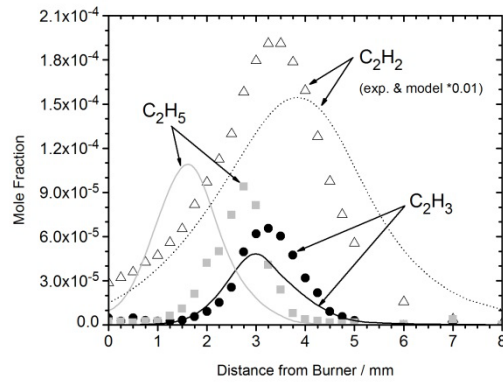
Comparison between experimental (symbols) and predicted (lines) species mole fraction profiles of educts and major products in Flame 2.

Figure 3: (134+10)x2.2=316+26=342 words



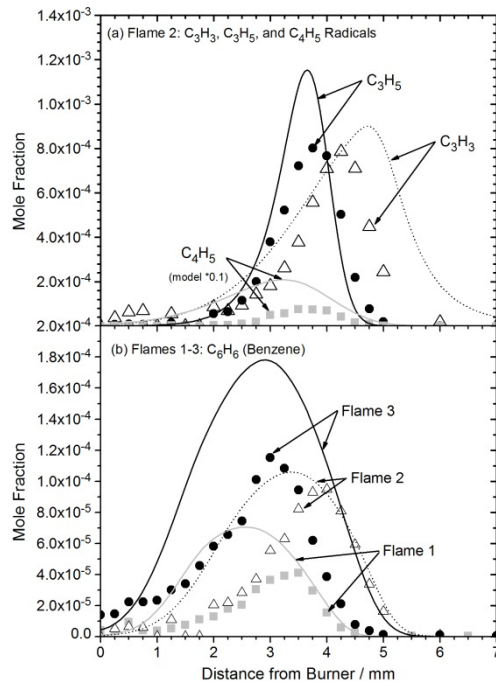
Comparison of experimental (symbols) and predicted (lines) mole fraction profiles of (a) CH₃, (b) C₂H₄, and (c) C₃H₄ (allene) for all three flames of this study.

Figure 4: (50+10)x2.2=128+35=165 words



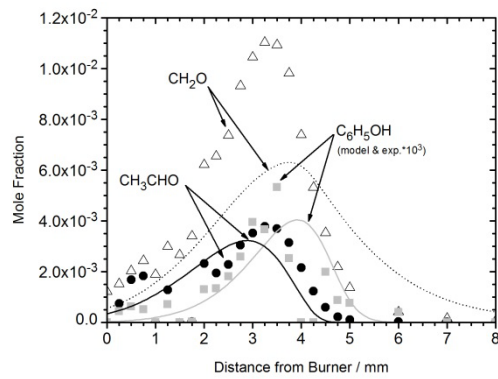
Comparison between experimental (symbols) and predicted (curves) species profiles in mole fraction of selected C_2H_x -species profiles of Flame 3: C_2H_2 , C_2H_3 , and C_2H_5 radicals. Experimental and modeling profiles of C_2H_2 have been multiplied by 0.01.

Figure 5: $(90+10) \times 2.2 = 220 + 26 = 246$ words



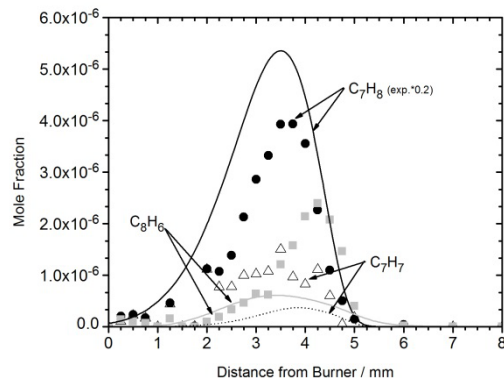
Experimental and modeled mole fraction profiles of (a) the benzene precursors C_3H_3 , C_3H_5 , and C_4H_5 in Flame 2 and (b) of benzene in all three flames.

Figure 6: (49+10)x2.2=130+33 = 163 words



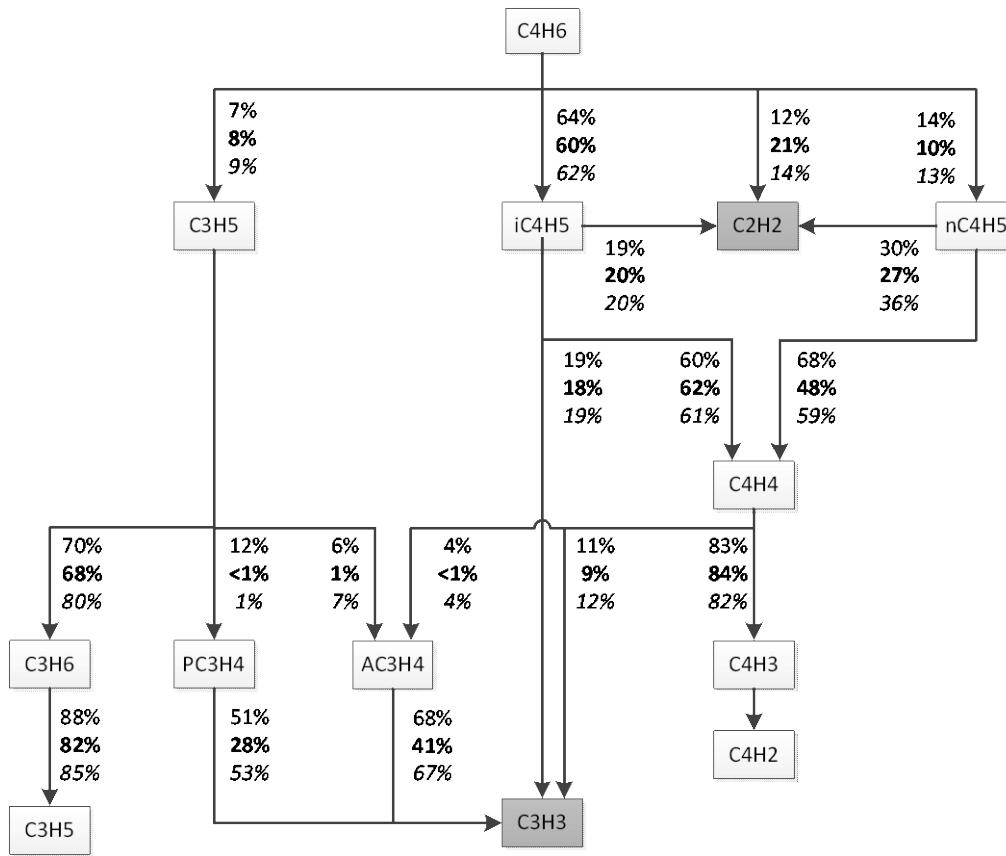
Comparison between experimental (symbols) and predicted (curves) species profiles in mole fraction for Flame 2: formaldehyde (CH_2O), acetaldehyde (CH_3CHO), and phenol ($\text{C}_6\text{H}_5\text{OH}$). Experimental and modeling profiles of $\text{C}_6\text{H}_5\text{OH}$ have been multiplied by 10^3 .

Figure 7: $(48+10) \times 2.2 = 128 + 26 = 154$ words



Comparison between experimental (symbols) and predicted (curves) species profiles in mole fraction of selected aromatic species for Flame 2: benzyl (C_7H_7), toluene (C_7H_8), and phenylacetylene (C_8H_6).

Figure 8: $(121+10) \times 2.2 \times 2 = 576 + 33 = 609$ words



Reaction path analysis for butadiene (C_4H_6) down to propargyl (C_3H_3) shown at 3 mm height above burner, for all three flames. Plain text: Flame 1; Bold text: Flame 2; Italic text: Flame 3.